Radiation Physics and Chemistry 168 (2020) 108549

Contents lists available at ScienceDirect

Radiation Physics and Chemistry

journal homepage: www.elsevier.com/locate/radphyschem

Application of artificial intelligence in scale thickness prediction on offshore petroleum using a gamma-ray densitometer

William L. Salgado[a], Roos Sophia de F. Dam[a], Tâmara P. Teixeira[a], C.C. Conti[b], C.M. Salgado[c,*]

[a] Universidade Federal do Rio de Janeiro, [PEN/COPPE-DNC/EE]CT, P.O. Box 68509, 21941-972, Rio de Janeiro, Brazil
[b] Instituto de Radioproteção e Dosimetria, CNEN/IRD, P.O. Box 37750, 22780-160, Rio de Janeiro, Brazil
[c] Instituto de Engenharia Nuclear, CNEN/IEN, P.O. Box 68550, 21945-970, Rio de Janeiro, Brazil

ARTICLE INFO

Keywords:
artificial neural network
Barium sulfate scale
Gamma densitometry
MCNP6 code
Oil pipelines

ABSTRACT

This work presents a methodology to study the deposition of scale in pipelines of multiphase systems (oil/water/gas), commonly found in the petroleum industry. The scale prediction for the pipelines is done through an artificial neural network, trained by using simulated data obtained with MCNP6 code, and transmission measurements. The model considered only barium sulfate ($BaSO_4$) as main scale's material. The transmission setup is composed of a ^{137}Cs (662 keV) volumetric source and one NaI(Tl) detector placed around the pipe. The pulse height distributions recorded in the detectors are used as input data of the artificial neural network. The results showed that 94% of the scale thickness prediction error was within ± 5%. The scale thickness in the oil industry's pipes can be calculated by the artificial neural network regardless of the presence of fluids with satisfactory results in water-gas-oil multiphase system with annular flow regime.

1. Introduction

In the oil industry, both oil and natural gas are the products of interest in the extraction from reservoir rocks. Nevertheless, three phases are involved in this process: liquid phases (oil and water); gas phase and; solid phase as sediment. Oil and gas extraction are accompanied by water and sludge and this mixture leads to the formation of deposits, scales, on the walls of the pipes and equipment. Scales cause the reduction of the its internal diameter, obstructing the passage of fluids, and demands periodic maintenance actions which increases costs (Candeias et al., 2014; Bahadori et al., 2013; Cowan and Weintritt, 1976). Besides all this, depending on the scales thickness, it may reduce the flow or, even, causes blockage in pipelines that may stop the production line (Coto et al., 2008). In addition to that, scale can cause corrosion in the pipeline, decreasing its life. The formation of insoluble scale types occurs when the injected seawater and formation waters are mixed in the reservoir, interacting chemically and precipitating minerals (Bahadori et al., 2013; Kamari et al., 2014). The formation of minerals deposits (scale) is caused by the precipitation of inorganic salts from produced water.

The scales are precipitated as a consequence of a disturbance in system pressures, temperatures and the mixing of waters with different chemical composition. Calcium carbonate scale is usually formed by the change of the pressure and temperature and it is also a function of composition and pipe inner surface properties (Zougari, 2010). Seawater contains considerable amounts of sulfate anions (SO_4^{2-}) while the formation water contains high concentration of divalent cations (calcium, strontium and barium). Therefore, the mix of injection and formation waters may lead to precipitation and the sulfate salts scale formation (Khatami et al., 2010; Bjørnstad and Stamatakis, 2006a).

Among the main scale associated with oil producing wells, barium sulfates ($BaSO_4$) stands out (Amiri and Moghadasi, 2010; Beserra, 2012; Bahadori et al., 2013; Oliveira et al., 2015; Teixeira et al., 2018; Zabihi et al., 2011).

Therefore, the scale is a very costly problem in oil and gas production operations. In this sense, there is a need for controlling the thickness of the scale for the assessment of preventive and corrective measurements without the need of stopping the plant operation.

Several papers have described both acoustic and non-acoustic methods for detecting the formation of scale in hydrocarbon wells. Acoustic methods are based on the reflection of acoustic signals and are possible to identify both type and thickness of the scale (Gunaratne and Keatch, 1996). On the other hand, some non-acoustic methods are based on monitoring pressure and temperature changes in certain parts of the plant, and only indicate the occurrence of a problem at an advanced stage.

* Corresponding author.
E-mail addresses: william.otero@hotmail.com (W.L. Salgado), rdam@nuclear.ufrj.br (R.S.d.F. Dam), tamarateixeira.eng@gmail.com (T.P. Teixeira), ccconti@ird.gov.br (C.C. Conti), otero@ien.gov.br (C.M. Salgado).

https://doi.org/10.1016/j.radphyschem.2019.108549
Received 7 August 2019; Received in revised form 18 September 2019; Accepted 27 October 2019
Available online 01 November 2019
0969-806X/

Nevertheless, in the context of non-acoustic methods, several radiation techniques have been used for scale detection in pipelines offshore applications using radiotracers (Bjornstad and Stamatakis, 2006b), neutrons (Abdul-Majid, 2013), computed radiography (Candeias et al., 2014) and gamma-ray densitometry (Monno, 1985; Oliveira et al., 2015; Teixeira et al., 2018).

Gamma-ray densitometry is very important in industry because it gives reliable data to accurate density fluctuation and, for this reason, has been investigated by many researchers. This methodology provides real time analysis and has proved to be an asset for flow measurement (Abouelwafa and Kendall, 1980; Bishop and James, 1992; Hussein and Han, 1995; Mi et al., 1997; Roshani et al., 2015, 2017a, 2017b, 2018; Salgado et al., 2009, 2010), thickness measurement (Berman and Harris, 1954), petroleum monitoring applications (Salgado et al., 2016; Khorsandi et al., 2013), gamma-ray scanning technique for troubleshooting analysis of column distillation (Buckley et al., 1985; Fulham and Hulbert, 1975), material's density prediction (Achmad and Hussein, 2004; Roshani et al., 2013; Salgado et al., 2016) and wall thickness pipes (Ramirez and Feliciano, 1992).

The determination of deposited scale is not an easy task because the presence of different types of fluids (gas, water, and oil), which interferes with the accuracy of the assessment of the scale thickness. Since the attenuation is predominated by Compton scatter and photoelectric. The cross-sections for both cases are proportional to the density of the materials.

Although the conventional sensors could perform a scale thickness measurement, it is expensive due to the installation and maintenance costs because of the direct contact of the sensor with the fluid, which can be abrasive, damaging the sensors, and need to be replaced periodically.

Among the nuclear techniques, the most common gamma-ray densitometry is based on transmission measurements of a gamma-ray beam to determine the density of the material. A radiation detector records the transmitted gamma-ray flux through the pipe's wall and the inner fluids.

The transmission measurement technique allows on-line monitoring the entire process with low cost and has shown to be a potential solution to the preventive control of scale (Bjørnstad and Stamatakis, 2006b; Oliveira et al., 2015; Teixeira et al., 2018). Furthermore, it is a noninvasive technique (the detector in a gamma-ray densitometry system is installed outside the pipe and is not in contact with the fluids), which can detect and quantify the scale with a single measurement geometry, without modifying the operational conditions.

A density calibration table may be performed by means of comparison of recorded counts by the detectors with the real density. However, this procedure can be influenced by significant parameters, depending on the measurement conditions or, even, errors in the calibration procedure itself (Johansen and Jackson, 2000). Furthermore, analytical equations are specific for a given geometry and flow regime and, obviously those parameters must not have considerable changes in order to attain reliable results.

In order to get over these problems, artificial neural networks (ANNs) have been used to interpret the pulse height distributions (PHDs) obtained by the gamma radiation detector (Salgado et al., 2016; Teixeira et al., 2018) for scale prediction. ANNs are mathematical models which has the ability of learning through examples and are able to detect patterns from a finite set of data. The ANN is able to generalize the knowledge acquired during the learning phase, to new input data that were not included in the training set but in the same search domain.

Due to the difficulties inherent to the collection of experimental data for the ANN training, the Monte Carlo N-Particle 6 (MCNP6) code (Pelowitz, 2013) was an asset for this work. The ideal and static theoretical models for annular regime have been developed using simulations by the Monte Carlo method to provide Training, Test and Validation data for the ANN. The MCNP6 code is used as a simulation tool for radiation transport and considers the main interactions of the radiation with all the materials involved in the setup.

Gamma-ray simulation with MCNP6 code comprises Rayleigh and Compton scattering, X-ray fluorescent emission, pair production and bremsstrahlung (Pelowitz, 2013). This code is applied to radioprotection, modeling of radiation detector, nuclear applications in the industry and so on. The models developed in the MCNP6 code, for this work, consider the main effects of interaction of radiation with matter involved and the PHDs from the NaI(Tl) scintillator detectors.

This is an upgrade of previous work, when the authors developed a methodology to calculate scale thickness using a geometry that consists of a 280 mm diameter steel tube containing barium sulfate scale ($BaSO_4$), a Cs^{137} gamma radiation source with narrow beam and a 2x2″ NaI(Tl) detector (Teixeira et al., 2018). The research was performed using the MCNPX code (Pelowitz, 2005) validated by means of analytical equations and compared with ANN. The input data of the ANN consisted of pipes with different internal diameters and many different scale thicknesses. The counts in the 662 keV energy photopeak were used to train the ANN and the flow investigated was just the oil (Teixeira et al., 2018). Meanwhile, this research presents a more realistic model to predict the concentric scale thickness in oil extraction pipeline that considers the influence of water-gas-oil on annular flow regime using the MCNP6 code (Pelowitz, 2013). Besides that, it was based on 1 ¾″x ¼″ scintillation detector that was validated experimentally (Salgado et al., 2012) and all pulse height distribution (PHD) obtained by the gamma radiation detector was used for pattern recognition by means of a trained ANN. Thus, this methodology is able to predict the scale thickness regardless of the presence of fluids inside the tube.

2. Methodology

The MCNP6 code is a simulation tool used for radiation transport, comprising: i) incoherent and coherent scattering; ii) the possibility of fluorescent emission after photoelectric absorption; iii) pair production with local emission of annihilation radiation and bremsstrahlung (Pelowitz, 2005). This technique is applied in the radiological protection, nuclear installations and modeling of radiation detectors.

In this work, MCNP6 code was used to simulate gamma-rays scattering and absorption from a radiation source in annular regime in an oil-water-gas pipeline. By the use of MCNP6 simulations, it was possible to generate an appropriated data set for training an ANN.

2.1. Detection geometry

The simulated setup consists of a 31.75 mm x 19.05 mm (1¼″ x ¾″) NaI(Tl) scintillator detector, positioned diametrically to a 662 keV collimated gamma-ray source of 8.84° divergence angle from a point source. A non-analog simulation was used to reduce the computing effort. The source emission directions were biasing to only those oriented toward the detector. Then a point source was collimated into a cone of directions using SI, SP and SB cards available on MCNP6. The gamma-ray PHDs acquired by the detector were directly used to feed an ANN. An iron tube composes a test section of 250 mm of outer diameter and 10 mm wall thickness. It includes a scale of barium sulfate ($BaSO_4$) of variable thickness and a gas, water and oil annular multiphase flow regime. The simulated setup is shown in Fig. 1 and has been used in previous works (Salgado et al., 2010, 2016).

A 3D view of the simulated system is shown in Fig. 2.

The simulations consisted of thirty two different scale thicknesses, varying from 0 mm (without scale) to 124 mm in steps of 4 mm. The volume fraction for the annular regime was 60% oil, 30% water and 10% gas that was chosen for a tube without scale and it was kept constant independently of the scales thickness, except for 124 mm of scale that represents a blockage tube. The $BaSO_4$ scale deposition considered in this work was a concentric ring geometry (McConn Jr.

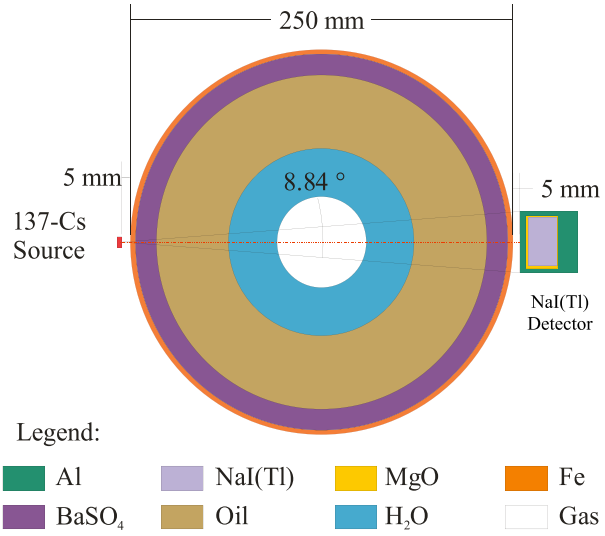

Fig. 1. Upper view cross section on simulated system.

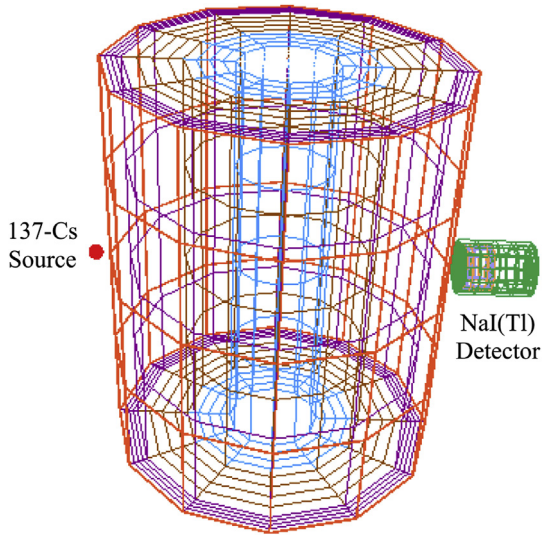

Figs. 2. 3D visualization of simulated system.

et al., 2011). The gaseous phase was substituted by air and oil was assumed as a hydrocarbon (molecular formula C_5H_{10}) with a 0.896 g. cm^{-3} density (Hussein and Han, 1995).

2.2. Material's linear attenuation coefficient

The attenuation coefficient for photoelectric effect at a given photon energy is highly dependent on both the atomic number and the density of the absorbing material (Knoll, 1989). Therefore, the method developed in this work, based on gamma-ray attenuation measurements, shows high sensitivity to the effective atomic number (Z) of the material and its density, mainly at low gamma-ray energies.

The linear attenuation coefficients for the barium sulfate and other materials used in this work can be determined by the transmission of a collimated mono-energetic beam by the Beer–Lambert's law, see Equation (1).

$$\mu_i = \frac{-\ln(I/I_o)}{x} \quad (1)$$

Where:

I: intensity of un-collided photons ($\gamma/cm^2.s$);
i: materials = wall pipe, scale, water, oil and gas;
I_o: intensity of primary photons ($\gamma/cm^2.s$);
μ: linear attenuation coefficient (1/cm);
x: beam path length through the absorber (cm).

The ANN training focus on density and thickness of absorber because the linear attenuation coefficient depends on these two variables to obtain the scale thickness. The linear attenuation coefficients for all the materials used in this work were calculated using a pencil beam point source, a surface detector and slab of the desired material (iron pipe, barium sulfate scale, water, gas and oil) in between. The linear attenuation coefficient was calculated by Equation (1) and required density ($g.cm^{-3}$) and weight fraction of materials used as input data for the MCNP6 code. The I/I_0 ratio was obtained using the current integrated over a surface detector by means of F1 tally card available in the code. The mass attenuation coefficient (μ/ρ) ($cm^2.g^{-1}$) was theoretically validated using data of the National Institute of Standards and Technology (NIST, 2018).

2.3. Detector simulation

The model of the NaI(Tl) detector considered the crystal as a homogeneous cylinder, with a MgO reflective layer and surrounded by an Al layer (Berger and Seltzer, 1972; Saito and Moriuchi, 1981; Salgado et al., 2012). The detector dimensions considered for the simulation was determined by the gammagraphy technique. The detector's crystal is 31 mm in diameter and 19 mm in thickness (Salgado et al., 2012).

The experimental absolute efficiency measurements for point sources (^{241}Am e ^{137}Cs) were compared with the simulated results under the same conditions of the experimental setup to validate the simulation of the NaI(Tl) detector. These sources were measured at a position source-detector distance of 5.45 cm, located on the longitudinal axis of the detector's crystal (Salgado et al., 2012).

The Gaussian energy broadening (GEB) of MCNPX code (card FTn) option was used. The deposited energy values are broadened by sampling from the Gaussian that approximates the energy resolution of the detector (Pelowitz, 2005). The GEB parameters were determined experimentally from the measurements of radioactive sources (Salgado et al., 2012). A non-linear function adjusted by least-squares procedure was applied to calculate the values of the "a", "b" and "c" coefficients, which will be used as input to the MCNPX code, using a fitting function shown in Equation (2) (Pelowitz, 2005).

$$FWHM = a + b\sqrt{E + cE^2} \quad (2)$$

Where:

E: incident gamma-ray energy (MeV);
a, b, c: user provided constants from the fitting function.

The F8 tally available in the MCNPX code provides the energy distribution of pulses created in a NaI(Tl) detector by radiation, which were used for the ANN training to predict the scale value. The energy bins accumulate the energy deposited in a cell by all the tracks of a photon. The F8 energy bins correspond to the total energy deposited in a detector in the specified channels by each photon (Pelowitz, 2005). Tally F8 scores Wc put in bin Ed pulses. Where: Wc - collective weight from a history for pulse height tally; Ed - total energy deposited by a history in a detector.

2.4. ANN training data

The main characteristic of the ANN is the ability of learning by examples. The ANN is able to discover behaviors and patterns from a finite set of data (called the "learning set"). This set is subdivided and

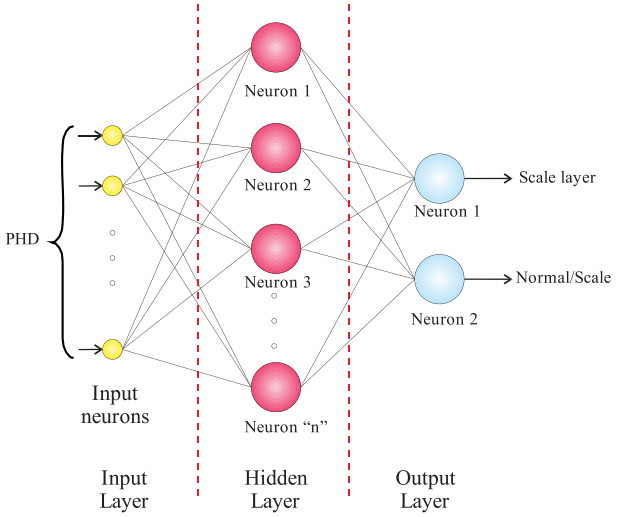

Fig. 3. Architecture for the proposed MLP model for thickness of scale prediction.

composed for training and test sets. The ANN is able to generalize the knowledge acquired during learning process and it may respond adequately to new situations. A third set (called the validation set) is used for a final test after ANN learning in order to assess ANN response under new data not included in the learning set. The simulations were performed for thirty two different scale thicknesses, varying from 0 mm to 124 mm in steps of 4 mm. These patterns were distributed uniformly throughout the search space. The 24 patterns training and 8 patterns test sets used to the network followed an approximate proportion of 70% and 30% respectively (Zadeh et al., 2016).

In this work, a 5-layer feed-forward multilayer perceptron (MLP) has been used and the test set was used for stopping criteria: cross validation in order to avoid over-training (Haykin, 1999). The learning algorithm was the back-propagation (Chauvin and Rumelhart, 1995). The proposed MLP model is shown in Fig. 3.

The simulated output of PHD was adjusted to the 20–800 keV energy range in steps of 10 keV and was used as the input for the 72 neurons ANN. The ANN is able to predict the condition of no scale, scale thickness equals zero. For this reason, the ANN has two outputs (2 neurons): i) the scale layer that record the thickness of layer, ii) normal/scale that represents (without scale) or with scale. If there is no scale, ANN output provides the value "0", but, if there is scale, the normal/scale output provides the value "1". For more information, the ANN input data is shown in Table 1.

The trained ANN was evaluated using another six patterns (validation set), varying from 2 mm to 22 mm in steps of 4 mm. These new patterns were also calculated by the MCNP6 code.

3. Results

The mass attenuation coefficient (μ/ρ), calculated from Equation (1), using the MCNP6 code was compared with the NIST data and the

Table 1
Detailed description of data formatting into the input of the ANN.

Pattern	PHDs					
P_1	$C_{20;1}$	$C_{30;1}$	$C_{40;1}$	–	$C_{710;1}$	$C_{720;1}$
P_2	$C_{20;2}$	$C_{30;2}$	$C_{40;2}$	–	$C_{710;2}$	$C_{720;2}$
–	–	–	–	–	–	–
P_{37}	$C_{20;37}$	$C_{20;37}$	$C_{40;37}$	–	$C_{710;37}$	$C_{720;37}$
P_{38}	$C_{20;38}$	$C_{20;38}$	$C_{40;38}$	–	$C_{710;38}$	$C_{720;38}$

*$C_{m;n}$: "m" = counts from channel and "n" = pattern.
Example: $C_{720;2}$ = counts record in channel 72 (720 keV) for pattern 2.

Table 2
The mass attenuation coefficient of different materials obtained using the MCNPX code and compared with NIST.

Material	Density ($g.cm^{-1}$)	μ: MCNP6 ($cm^2.g^{-1}$)	μ: NIST ($cm^2.g^{-1}$)	Error (%)
Iron	7.874	7.2136E-2	7.3460E-2	1.84
Water	1.0	8.5193E-2	8.5740E-2	0.64
Oil	0.896	8.7710E-2	8.8807E-2	0.41
Gas	1.205E-3	7.6362E-2	7.7130E-2	1.00
Barium sulfate	4.5	7.5157E-2	7.7500E-2	3.12

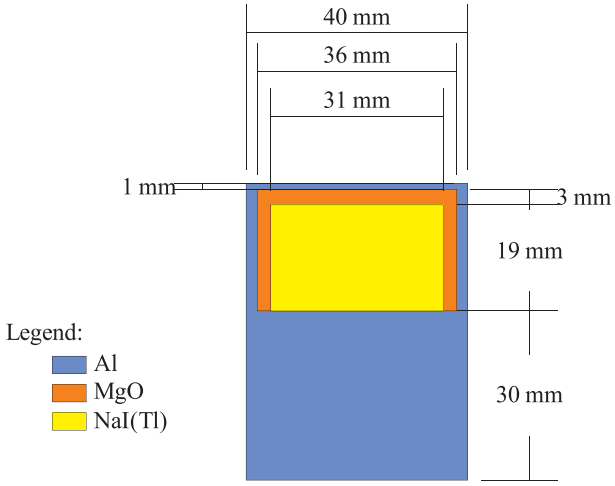

Fig. 4. Schematic representation of the NaI(Tl) detector considered in simulation.

results are shown in Table 2. These data were used for calculating the scale thickness.

The comparison showed a relative error less than 4%, indicating that the models developed in the MCNP6 code are reliable and can be used in the training of ANN.

The detector's simulation was validated both qualitatively by the energy resolution curve and quantitatively by the photon detection efficiency. The NaI(Tl) detector's model (regions, material and dimensions) considered for purposes of calculating with the MCNP6 code is shown in the Fig. 4 (Salgado et al., 2012), and Fig. 5 shows the comparison between the experimental and simulated spectra for the 662 keV gamma-ray flux of the ^{137}Cs point source.

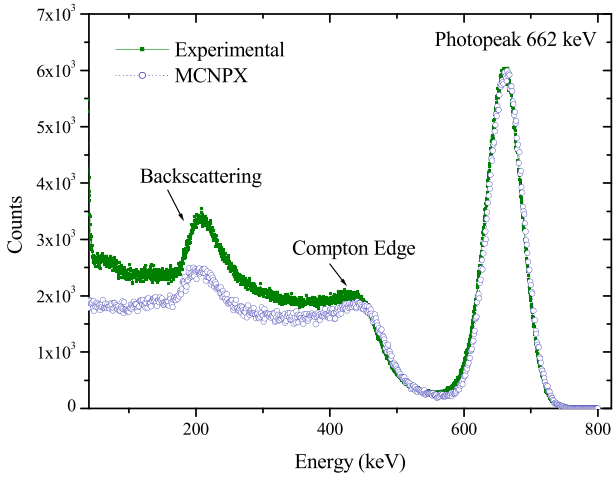

Fig. 5. Comparison between experimental and simulated pulse height distributions to ^{137}Cs source.

There is an acceptable agreement in the full photopeak area, but, for the Compton continuum below 400 keV, the concordance is a little lower than the experimental data due to scattering on the detector's shielding, support and surrounding materials (Berger and Seltzer, 1972). The technique of the "shadow shield" can minimize these differences (Sima, 1990; Conti et al., 1999). Compared to the experimental data, a small discrepancy can be seen because the effect of scintillation efficiency increases in the low-energy region where scintillation efficiency is nonlinear and is not considered in the MCNP6 code. It is also due to the low precision of low energy electron cross-section.

An arbitrary scaling of data in order to match the experimental and simulated spectra were used from by the counts in the maximum height of the full photopeak of ^{137}Cs that was multiplied by counts normalized (per source particle) from MCNP6 code. The adjustment coefficients of energy resolution for the NaI(Tl) detector, a = 0.0024, b = 0.05165 and c = 2.85838, were obtained after adjusting a function provided by Equation 3 (Salgado et al., 2012).

The 2E8 number per stories (NPS) was determined to obtain the relative error below 10% for all range energy, except for the full photopeak area that was 1%.

Fig. 6 presents the expected results, from the MCNP6 code, for some different thickness of scale for a volume fraction of 60% oil, 30% water and 10% gas for annular regime. It is worth mentioning that the X-ray of the K shell of $^{137m}Ba_{56}$ ($BaK\alpha_1$) was not considered in the simulation because it plays no role in the process.

The data from the scale predicted by the ANN were fit to a linear equation by the least-squares procedure and the linear correlation coefficient showed to be of 0.99996. A good agreement between the scale thickness predicted by the ANN and the scale thickness considered in the simulations shows the ability of generalization of the network. The values predicted by the ANN for scale thickness were close to the thickness considered in the simulations and are showed in the Fig. 7.

It can be observed that the ANN could adequately predict the scales even when the volume of the material is modified due to the smaller diameter of the pipe caused by the scale.

The results obtained for the validation set (6 patterns) are shown in Table 3 and indicate that the ANN could adequately predict the scale thickness.

Once the ANN is trained and validated for a given geometry, it can be used for scale thickness determination without any further adjustment for the on-line measurements. The results show a good performance of the trained ANN, mainly for patterns not used in the learning phase, pointing that the ANN could predict the scale thickness, regardless of variations in fluid volume.

The mean relative error (MRE) and root mean squared error (RMSE) have been calculated to evaluate the network. The error values for scale thickness for the Training (TRT), Test (TST), and Validation (VAL) sets are shown in Table 4. The results demonstrate a good convergence of ANNs about all data set in densities prediction.

The ANN could predict the scale thickness within 10% of error and more than 94% of the cases were less than 5%. The ANN performance of the thickness of scale predictions is summarized in Table 5.

It was possible to design one ANN based on the differences between the PHDs for the scale thickness with good results for all the patterns. The ANN was able to correctly identify the presence of scale and, even,

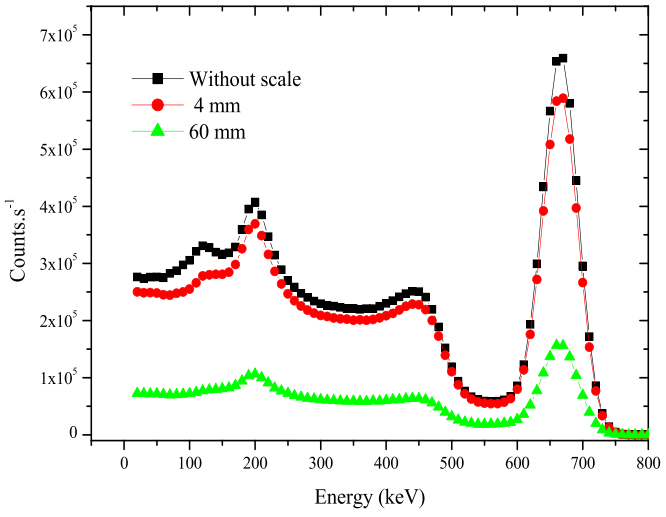

Fig. 6. The PHDs for different thickness of scale for beam transmitted.

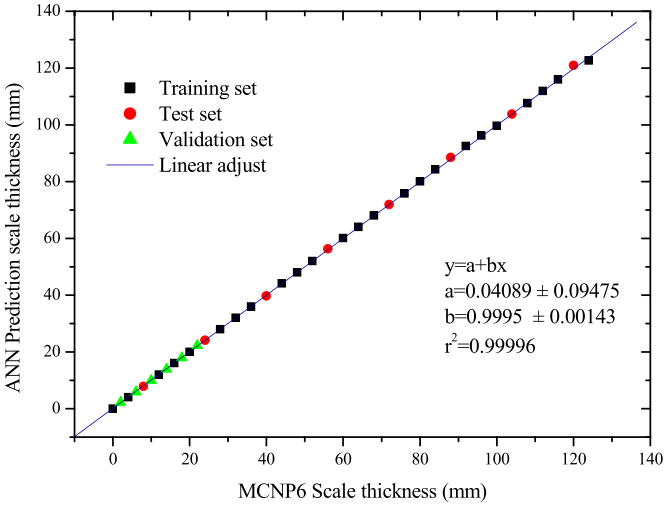

Fig. 7. Results obtained for all sets.

Table 3
ANN prediction for the validation set.

Scale thickness (mm)		Absolute Error	Relative Error (%)
Real (MCNP6)	Predicted (ANN)		
2	2.18	-0.18	-9.00
6	5.91	0.09	1.50
10	9.93	0.07	0.70
14	13.99	0.01	0.07
18	17.88	0.12	0.67
22	22.18	-0.18	-0.82

Table 4
The obtained errors for Training, Test and Validation sets of the proposed ANN model.

Sets	Scale Thickness	
	MRE(%)	RMSE
TRT	0.16	0.31
TST	0.63	0.43
VAL	2.54	0.14
TOTAL	0.60	0.09

Table 5
Summary of pattern recognition for the prediction results.

Probability of correct rating	Scale Thickness
≤5%	94.737
5%–10%	2.632
10%–20%	0
20%–30%	0
> 30%	0
r^2	0.99996

in the case of no scale.

The Intel® Core™ I7-8700 CPU @ 3.20 GHz and 32.0 GB of RAM computer was used to run MCNP6 on 64 bit windows operating system and train the ANN. Each pattern spent an average of around of 50 min to run the MCNP6 code with 2E8 NPS and 2 min to training of the ANN.

4. Conclusions

This work was intended to investigate the response of multiphase flow systems to gamma-ray transmission detection in order to predict the scale thickness regardless of the fluids proportions. The proposed approach is based on PHDs pattern recognition by means of a trained ANN with data generated by the MCNP6 Monte Carlo code. The good results for all patterns presented maximum relative error of 0.60%. 94% of the test data were predicted with relative error below ± 5%. The results indicate that the methodology can be used since the proposed ANNs could correctly predict the scale thickness with satisfactory results in water-gas-oil multiphase system. In the proposed approach, it is important to note that no prior knowledge about the presence of fluids and the fractions is needed if the neural network is properly trained. The system is still able to predict whether or not there is scale.

Acknowledgements

The authors gratefully acknowledge the financial support from the Coordenação de Aperfeiçoamento de Pessoal de Nível Superior (CAPES) of Brazil and Comissão Nacional de Energia Nuclear (CNEN) of Brazil. Thanks are also to Instituto de Engenharia Nuclear (IEN).

Appendix A. Supplementary data

Supplementary data to this article can be found online at https://doi.org/10.1016/j.radphyschem.2019.108549.

References

Abdul-Majid, S., 2013. Determination of wax deposition and corrosion in pipelines by neutron back diffusion collimation and neutron capture gamma-rays. Appl. Radiat. Isot. 74, 102–108.
Abouelwafa, M.S.A., Kendall, E.J.M., 1980. The measurement of component ratios in multiphase systems using gamma-ray attenuation. J. Phys. E Sci. Instrum. 13, 341–345.
Achmad, B., Hussein, E.M.A., 2004. An X-ray Compton scatter method for density measurement at a point within an object. Appl. Radiat. Isot. 60, 805–814.
Amiri, M., Moghadasi, J., 2010. Prediction the amount of Barium Sulfate scale formation in Siri oilfield using OLI ScaleChem software. Asian Journal of Scientific Research 3 (4), 230–239.
Bahadori, A., Zahedi, G., Zendehboudi, S., 2013. Estimation of potential barium sulfate (barite) precipitation in oilfield brines using a simple predictive tool. Environ. Prog. Sustain. Energy 32, 860–865.
Berger, M.J., Seltzer, S.M., 1972. Response functions for sodium iodide scintillation detectors. Nucl. Instrum. Methods 104, 317–332.
Berman, A.I., Harris, J.N., 1954. Precision measurement of uniformity of materials by gamma-ray transmission. Rev. Sci. Instrum. 25 (1), 21–29 (January).
Beserra, M.T.F., 2012. Avaliação da espessura de incrustações em dutos de extração de petróleo. M.S. thesis. Instituto de Radioproteção e Dosimetria, Rio de Janeiro, RJ, Brasil.
Bishop, C.M., James, G.D., 1992. Analysis of multiphase flows using dual-energy gamma densitometry and neural networks. Nucl. Instrum. Methods 327–580.
Bjørnstad, T., Stamatakis, E., 2006b. Applicability and Sensitivity of Gamma Transmission and Radiotracer Techniques for Mineral Scaling Studies. Institute for Mineral Scaling Studies, Institute for Energy Technology, NORWAY.
Bjørnstad, T., Stamatakis, E., 2006a. Scaling studies with gamma transmission technique. Oilfield Chem. 19–22 March 2006, Geilo, NORWAY.
Buckley, P.S., Luyben, W.L., Shunta, J.P., 1985. Design of Distillation Column Control Systems. Edward Arnold.
Candeias, J.P., Oliveira, D.F., Anjos, M.J., Lopes, R.T., 2014. Scale analysis using X-ray microfluorescence and computed radiography. Radiat. Phys. Chem. 95, 408–411.
Chauvin, Y., Rumelhart, D.E., 1995. Backpropagation Theory, Architectures and Applications.
Conti, C.C., Sachet, I.A., Bertelli, L., Lopes, R.T., 1999. Ge detectors calibration procedure at IEN/CNEN for in situ measurements. In: II International Symposium on Technologically Enhanced Natural Radiation, (Rio de Janeiro).
Coto, B., Martos, C., Peña, J.L., Espada, J.J., Robustillo, M.D., 2008. A new method for determination of wax precipitation from non-diluted oils by fractional precipitation. Fuel 87, 2090–2094.
Cowan, J.C., Weintritt, D.J., 1976. Water-Formed Scale Deposits, in Water-Formed Scale Deposits. Gulf Publishing, Houston, Tex, USA, pp. 97–108.
Fulham, M.J., Hulbert, V.G., 1975. Gamma scanning of large towers. Chem. Eng. Prog. 71, 73–77.
Gunaratne, G.P.P., Keatch, R.W., 1996. Novel techniques for monitoring and enhancing dissolution of mineral deposits in petroleum pipelines. Ultrasonics 34 (2–5), 411–419.
Haykin, S., 1999. Neural Networks, second ed. A Comprehensive Foundation, Hamilton, Ontario, Canada Prentice-Hall.
Hussein, E.M.A., Han, P., 1995. Phase volume-fraction measurement in oil-water-gas flow using fast neutrons. Nucl. Geophys. 9 (3), 229–234.
Johansen, G.A., Jackson, P., 2000. Salinity independent measurement of gas volume fraction in oil/gas/water pipe flows. Appl. Radiat. Isot. 53, 595–601.
Kamari, A., Gharagheizi, F., Bahadori, A., Mohammadi, A.H., 2014. Rigorous modeling for prediction of barium sulfate (barite) deposition in oilfield brines. Fluid Phase Equilib. 366, 117–125.
Khatami, H.R., Ranjbar, M., Schaffie, M., Emady, M.A., 2010. Development of a fuzzy saturation index for sulfate scale prediction. J. Pet. Sci. Eng. 71, 13–18.
Khorsandi, M., Feghhi, S.A.H., Salehizadeh, A., Roshani, G.H., 2013. Developing a gamma-ray fluid densitometer in petroleum products monitoring applications using artificial neural network. Radiat. Meas. 59, 103–187.
Knoll, G.F., 1989. Radiation Detection and Measurement, second ed. John Wiley & Sons, Inc., pp. 51–52.
McConn Jr., R.J., Gesh, C.J., Pagh, R.T., Rucker, R.A., Williams III, R.G., 2011. "Compendium of Material Composition Data for Radiation Transport Modeling". Radiation Portal Monitor Project, Pacific Northwest. National Laboratory PIET-43741-TM-963 PNNL-15870 Rev. 1.
Mi, Y., Tsoukalas, L.H., Ishii and, M., 1997. Application of multiple self-organizing neural networks: flow pattern classification. Trans. Am. Nucl. Soc. 77, 114–116.
Monno, A., 1985. "Tube wall thickness" GB patent document 2146115/A/, GB patent application 8323913. G01B 15/02. Int. Classif. 9 April).
NIST, August 22, 2018. [Online]. Available. https://physics.nist.gov/cgi-bin/Xcom/xcom2.
Oliveira, D.F., Nascimento, J.R., Marinho, C.A., Lopes, R.T., 2015. Gamma transmission system for detection of scale in oil exploration pipelines. Nucl. Instrum. Methods Phys. Res., Sect. A 784, 616–620.
Pelowitz, D.B., 2005. "MCNPX TM User's Manual" Version 2.5.0, LA-CP-05-0369. Los Alamos National Laboratory.
Pelowitz, D.B., 2013. "MCNP6 TM User's Manual", Version 1.0, LA-CP-13-00634, Rev. 0. Los Alamos National Laboratory, USA.
Ramirez, G.F., Feliciano, H.J., 1992. Methodology to calculate wall thickness in metallic pipes. Salazar (Mexico) In: 6° Seminar of the IIE-INIM-IMP on Technological Specialities, pp. 15 (July).
Roshani, G.H., Nazemi, E., Roshani, M.M., 2017a. A novel method for flow pattern identification in unstable operational conditions using gamma ray and radial basis function. Appl. Radiat. Isot. 123, 60–68.
Roshani, G.H., Feghhi, S.A.H., Adineh-Vand, A., Khorsandi, M., 2013. Application of adaptive neuro-fuzzy inference system in prediction of fluid density for a gamma-ray densitometer in petroleum products monitoring. Measurement 46, 3276–3281.
Roshani, G.H., Karami, A., Khazaei, A., Olfateh, A., Nazemi, E., Omidi, M., 2018. Optimization of radioactive sources to achieve the highest precision in three-phase flow meters using Jaya algorithm. Appl. Radiat. Isot. 139, 256–265.
Roshani, G.H., Karami, A., Salehizadeh, A., Nazemi, E., 2017b. The capability of radial basis function to forecast the volume fractions of the annular three-phase flow of gas-oil-water. Appl. Radiat. Isot. 129, 156–162.
Roshani, G.H., Nazemi, E., Feghhi, S.A.H., 2015. Flow regime identification and void fraction prediction in two-phase flows based on gamma ray attenuation. Measurement 62, 25–32.
Saito, K., Moriuchi, S., 1981. Monte Carlo calculation of accurate response functions for a NaI(Tl) detector for gamma-rays. Nucl. Instrum. Methods 185, 299–308.
Salgado, C.M., Brandão, L.E.B., Conti, C.C., Salgado, W.L., 2016. Density prediction for petroleum and derivatives by gamma-ray attenuation and artificial neural networks. Appl. Radiat. Isot. 143–149.
Salgado, C.M., Brandão, L.E.B., Schirru, R., Pereira, C.M.N.A., Silva, A.X., Ramos, R., 2009. Prediction of volume fractions in three-phase flows using nuclear technique and artificial neural network. Appl. Radiat. Isot. 67, 1812–1818.
Salgado, C.M., Brandão, L.E.B., Schirru, R., Pereira, C.M.N.A., Conti, C.C., 2012. Validation of a NaI(Tl) detector's model developed with MCNPX code. Prog. Nucl. Energy 59, 19–25.
Salgado, C.M., Pereira, C.M.N.A., Schirru, R., Brandão, L.E.B., 2010. Flow regime identification and volume fraction prediction in multiphase flows by means of gamma-ray attenuation and artificial neural networks. Prog. Nucl. Energy 52 (6), 555–562.
Sima, O., 1990. Monte Carlo simulation versus semiempirical calculation of auto absorption factors for semiconductor detector calibration in complex geometries. Prog. Nucl. Energy 24, 327–336.
Teixeira, T.P., Salgado, C.M., Dam, R.S.F., Salgado, W.L., 2018. Inorganic scale thickness prediction in oil pipelines by gamma-ray attenuation and artificial neural network. Appl. Radiat. Isot. 141, 44–50.
Zabihi, R., Schaffie, M., Nezamabadi-Pour, H., Ranjbar, M., 2011. Artificial neural network for permeability damage prediction due to sulfate scaling. J. Pet. Sci. Eng. 78 (3–4), 575–581.
Zadeh, E.E., Feghhi, S.A.H., Roshani, G.H., Rezaei, A., 2016. Application of artificial neural network in precise prediction of cement elements percentages based on the neutron activation analysis. Eur. Phys. J. Plus 131. https://doi.org/10.1140/epjp/i2016-16167-6.
Zougari, M.I., 2010. Shear-driven crude oil wax deposition evaluation. J. Pet. Sci. Eng. 70, 28–34.